

Article

Compositional Variations of Cr-Spinel in High-Mg Intrusions of the Primorsky Ridge (Western Baikal Region, Russia)

Aleksey S. Mekhonoshin , Tatiana B. Kolotilina , Artemy A. Doroshkov and Evgeniya E. Pikiner

A.P. Vinogradov Institute of Geochemistry Siberian Branch, Russian Academy of Science, 664033 Irkutsk, Russia; tak@igc.irk.ru (T.B.K.); artemiy@igc.irk.ru (A.A.D.); e.pikiner@igc.irk.ru (E.E.P.)

* Correspondence: mekhonos@igc.irk.ru; Tel.: +7-3952-42-4601

Received: 19 May 2020; Accepted: 3 July 2020; Published: 7 July 2020



Abstract: Composition variations of Cr-spinel in high-Mg rocks of the Primorsky Ridge (Western Baikal region, Russia) are reported here. A specific feature of Cr-spinels in ultramafic rocks of the Primorsky Ridge is their noticeably high Ti content (up to 6.5 wt.%) compared to spinels in mantle peridotites. The presence of high TiO₂ content in Cr-spinels enclosed in olivine crystals may be a clear indication of the primary magmatic nature of Ti enrichment. Two types of Cr-spinel were identified in ultramafic rocks from all intrusions. Cr-spinels of Type I are enclosed in the inner part of olivine crystals and are homogeneous Al-rich chromites and Fe²⁺-rich chromites. They are characterized by variable content of TiO₂ (1.0–5.3 wt.%), moderately high Cr# (0.7–0.83), and low Fe³⁺# (0.20–0.34). Cr-spinels of type II occur in the interstitial space and occur as homogeneous and zoned grains with Al-rich chromite and Fe²⁺-rich chromite cores. Al-rich chromite cores have a composition similar to that of the Cr-spinel enclosed in olivine crystals. Fe²⁺-rich chromite cores have relatively high MgO (3.8–6.2 wt.%), Al₂O₃ (8–9 wt.%), and TiO₂ (2.6–2.8 wt.%) content, low MnO (0.34–0.52 wt.%) content, and a low Fe³⁺# (0.25–0.27) ratio.

Keywords: Cr-spinel; Ti content; high-Mg rocks; large igneous province; Siberian craton basement; Russia

1. Introduction

Chromian spinel is an important petrogenetic [1–6] and tectonic setting [5,7–9] indicator in ultramafic and mafic rocks. The cation (Cr, Al, Fe²⁺, Fe³⁺, Ti) ratios in chromian spinel change according to physical and chemical conditions [2,3,6,10]. Even though subsolidus reequilibration and/or metamorphism could modify the primary composition of chromian spinel [3,11–15], liquidus spinel can trace the composition of a differentiating magmatic liquid and allows the evaluation of parental magma conditions [4,7,10,16,17]. Conversely, the original chemistry of altered or metamorphosed rocks can be estimated from the relict chromian spinel [4,5,18].

In southern Siberia, Precambrian ultramafic complexes are represented by Neoproterozoic dunite-peridotite-pyroxenite-gabbro intrusions in the mobile belts surrounding the Siberian craton and Meso- and Paleoproterozoic plagioperidotite-gabbroic intrusions in the Sharyzhalgai uplift of the Siberian craton basement [19]. In the western Baikal region, there is a Neoproterozoic Ioko-Dovyren mafic-ultramafic pluton [20] in the Olokit zone on the Siberian cratonic margin to the north of Lake Baikal. In addition, ultramafic intrusions in this region are localized in structures of the southwestern part of the Baikal cratonic basement uplift (Figure 1a). Until recently, there was no information about the age or the petrographical, geochemical, and mineralogical features of these ultramafic rocks.

Limited information on the subject is available in the explanatory note for the State geological map of Russia, which mentions their ultrabasic composition.

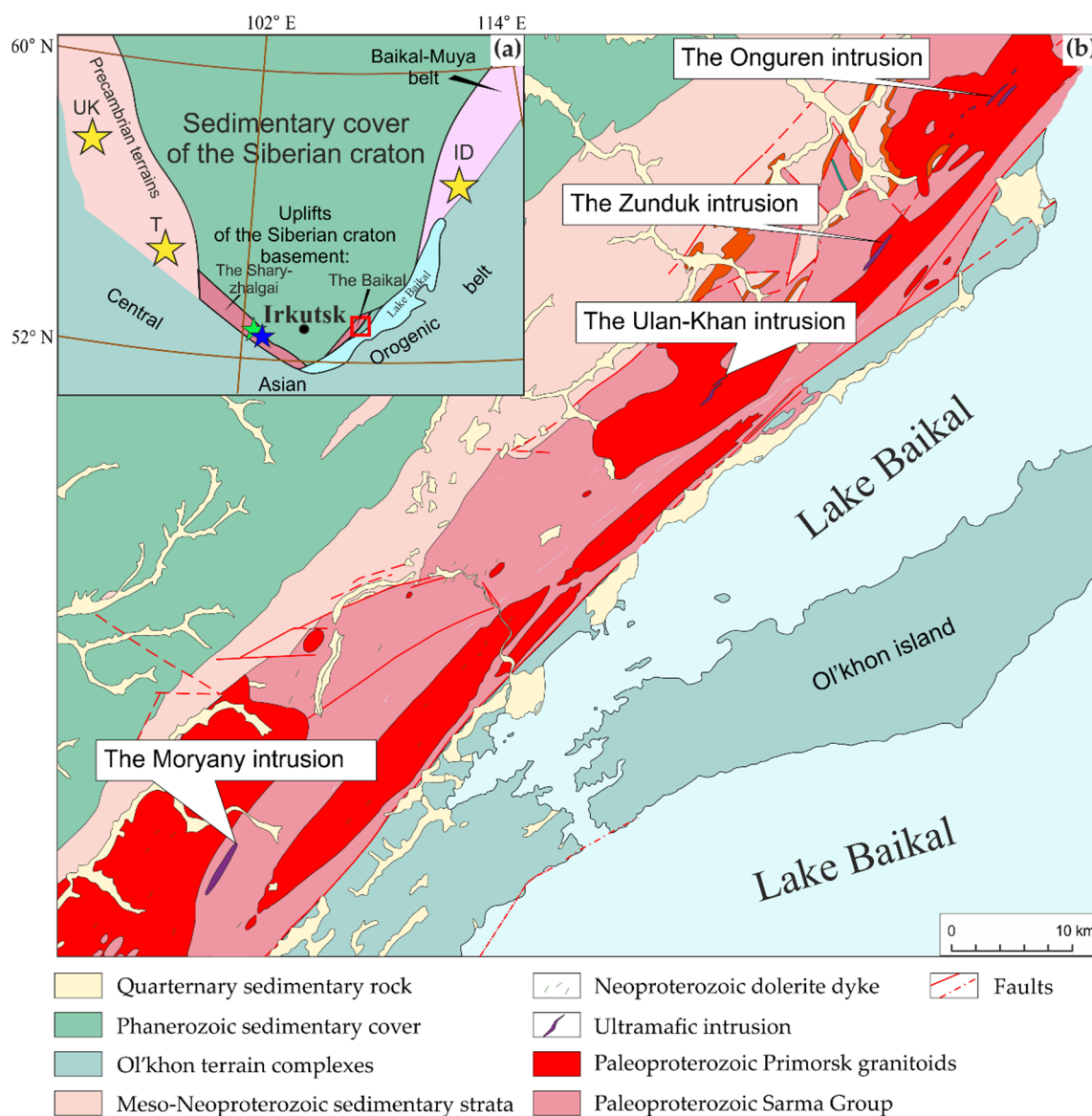


Figure 1. (a) Sketch of the tectonic map of southern Siberia and the location of the region where the studied ultramafic intrusions are located (red square). Stars indicate the locations of the Precambrian mafic-ultramafic intrusions: yellow—Neoproterozoic (UK—Upper Kingash, T—Tartay, Medek, etc., ID—Ioko-Dovyren), blue—Mesoproterozoic (Srednecheremshanka), green—Paleoproterozoic (Malyi Zadoi); (b) Simplified geological map of the southwestern part of the Akitkan orogenic belt and adjacent areas.

The distribution of the Neoproterozoic intrusions that occur along two distinct trends, northwest and northeast, along the margins of the Irkutsk Promontory (Figure 1a) may indicate that these are part of a radiating triple junction system related to Large Igneous Province (LIP) magmatism [21]. The high-Mg intrusion of the Primorsky Ridge could be considered as the “missing link” in the Precambrian ultrabasic magmatism of this region. Our field observations, along with textural (Figure 2) and mineralogical features, identify these as Neoproterozoic hypabyssal intrusions [22]. They are characterized by high-Mg bulk composition, light-rare earth element-enriched patterns, and the presence of sulfide and platinum-group minerals [22,23].

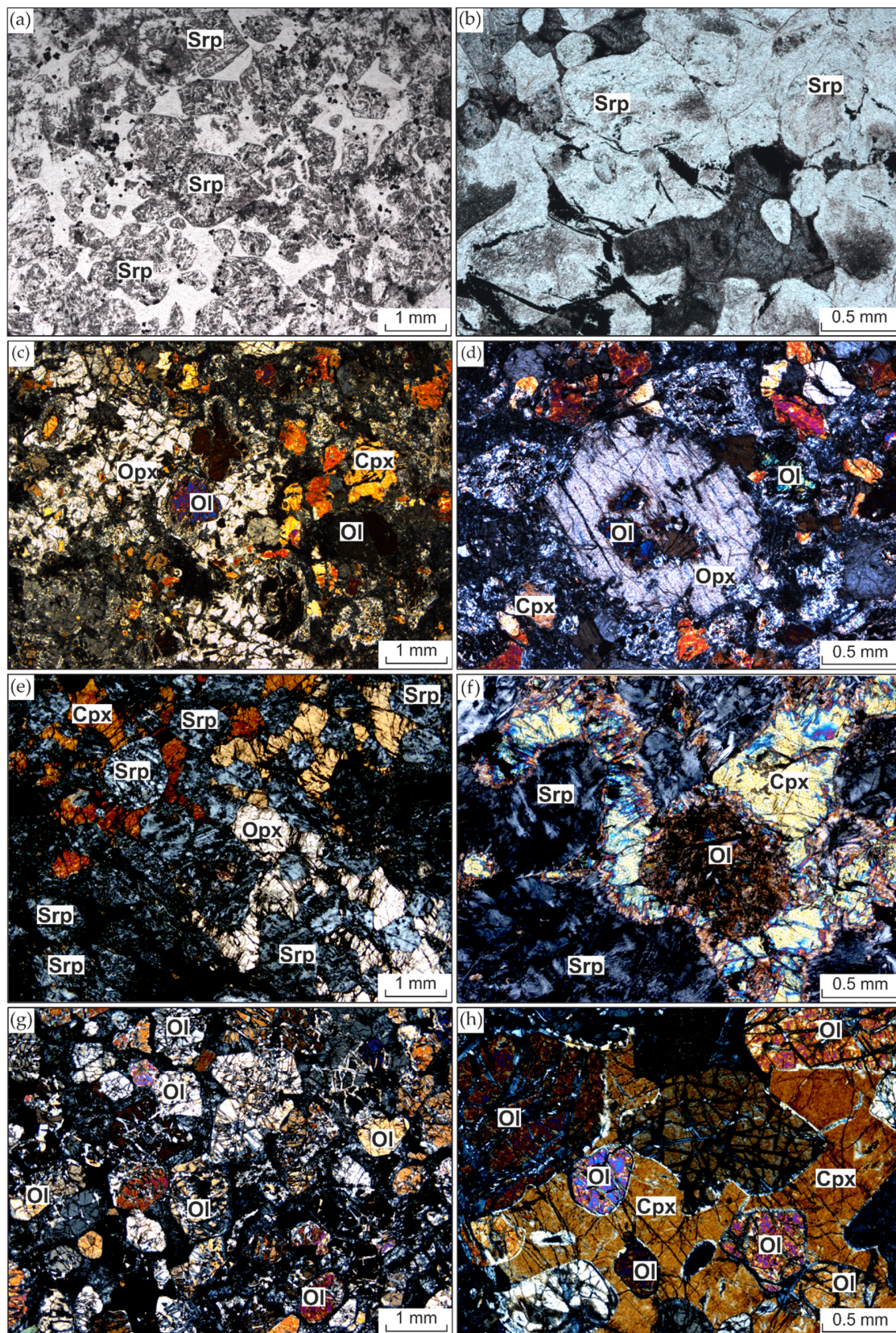


Figure 2. Photomicrographs showing textural characteristics: (a,b) The Moryany intrusion; (c,d) The Ulan-Khan intrusion; (e,f) The Zunduk intrusion; (g,h) The Onguren intrusion. (a,b) Plane-polarized light; (c-h) Cross-polarized light. Ol: olivine; Opx: orthopyroxene; Cpx: clinopyroxene; Srp: serpentine.

Detailed mineralogical studies of these rocks have not yet been conducted. The main goal of this work is to study the genesis of Cr-spinel from high-Mg intrusions of the Primorsky Ridge using new compositional data. Analyzed Cr-spinels are characterized by high TiO₂ content (up to 6.5 wt.%) and distinct core-to-rim zoning. Although most of the Cr-spinel grains in these rocks were altered, the grains encased in olivine were used to obtain information about the primary composition of the Cr-spinels. In addition, comparison of the obtained data on core and rim parts allowed us to understand the processes of evolution and alteration in the composition of Cr-spinels in the ultramafic rocks of the Primorsky Ridge.

2. Materials and Methods

In this research, we studied the rock samples collected from a rock outcrop. The analyses were carried out at the Common Use Center of Isotope and Geochemical Studies in the Vinogradov Institute of Geochemistry, Irkutsk, Russia. Whole-rock major elements and Ni and Cr were analyzed by an S4 Pioneer X-ray fluorescence (XRF) spectrometer (Bruker AXS, Karlsruhe, Germany). Determination of FeO was performed by the titrimetric bichromatic method from solutions after acid dissolution of samples. K, Ti, and trace elements were analyzed by inductively coupled plasma mass spectrometry (ICP-MS) using an Element 2 mass spectrometer (FinniganMAT, Bremen, Germany) with double-focusing and registration of the signal in three resolutions: low (LR)-300, middle (MR)-4000, and high (HR)-10000 M/ΔM. The analyses were performed under standard operating conditions. The accuracy of the determination of trace element concentrations and the drift of the device were controlled using international reference samples of SDU-1 dunite and JP-1 peridotite. Corresponding errors for XRF and ICP-MS analyses were within 5%.

Composition of minerals was determined *in situ* from polished thin sections of all samples. They were analyzed on a JEOL JXA8200 SuperProbe (JEOL, Tokyo, Japan), a high-resolution SEM and WD/ED Combined Electron Probe Microanalyzer equipped with a five-wavelength dispersive X-ray spectrometer, and an energy dispersive X-ray spectrometer with a 133 eV lithium drift type silicon semiconductor detector. Elements were determined by their characteristic X-ray wavelengths on wave-dispersion spectrometers, at the following operation conditions: accelerating voltage 20 kV, beam current 20 nA, beam diameter 1 μm, and count time of 10 s along the peak line plus 5 s for the background on both sides of the peak line. Proprietary software was used for data processing. Metrological characteristics of the analytical technique [24,25] were determined on control samples of known composition.

FeO and Fe₂O₃ content in the Cr-spinels were estimated using spinel stoichiometry after subtraction of the ulvospinel component, corresponding to the TiO₂ content. The deficit of trivalent (Cr, Al, Ti, V) cations in relation to divalent (Fe, Mg) was computed after calculating the molar percentage of each element. The Fe₂O₃ content was subtracted from the total FeO to obtain the factual FeO content.

3. Geological Background

The Siberian craton was assembled between 2.1 and 1.8 Ga through multiple collisions of four Archaean (Tungus, Anabar, Aldan, Stanovoy) and one Palaeoproterozoic (Olenek) superterraces [26,27]. The Late Palaeoproterozoic Akitkan orogenic belt (Figure 1b) separates the Aldan and Anabar superterraces [26,27]. A large part of the Siberian craton is covered by Mesoproterozoic-Neoproterozoic and Phanerozoic sediments, with only a few exposed crystalline basement areas (Figure 1a). The Precambrian basement of the southern part of the Siberian craton is exposed in narrow uplifts bounded by deep fault zones. The Baikal Precambrian uplift is part of the ~2.0–1.8 Ga Akitkan orogenic belt [26,27]. Paleoproterozoic metamorphic complexes of the Baikal uplift are combined into the Sarma Group in the south and into the Chuya Group in the north. They are composed of greenschist- and granulite-facies metamorphic rocks [28]. Foliated granitoids are widespread in this area and were previously considered to have formed prior to or during the ~1.9 Ga accretional and collisional events

in the region [27]. Metamorphic complexes are intruded by the unmetamorphosed 1.87–1.85 Ga post-collisional Primorsk granitoids [29].

Studied ultramafic intrusions are located in the southwestern part of the Baikal uplift of the Siberian craton basement (Figure 1b). In orographic terms, this part of the uplift belongs to the mid-altitude mountain ridge—Primorsky. The topography of the Primorsky Ridge in this area is gradually increasing and reaches an average of about 900–1100 to 1400 m (Figure S1).

Ultramafic bodies occur in the four locations and are exposed in a series of hypabyssal intrusions oriented in a northeastern direction (Figure 1b). In each location, there are several steeply dipping lenticular or dyke-like bodies, intersecting metamorphic rocks of the Sarma Group and granitoids of the Paleoproterozoic Primorsk complex (Figures S2 and S3). Numerous Neoproterozoic [30,31] dolerite dykes are often spatially associated with ultramafic intrusions. Widths of the ultramafic outcrops are 50–200 m, with lengths of up to 2 km. In the Moriany intrusion, only large blocks of rock can be found in the field, distributed over the former outcrop area of the dykes (Figure S4).

These rocks can be divided into two types based on their texture and olivine compositions. The first type is characterized by a porphyritic texture with zoned olivine phenocrysts (the Moriany and Ulan-Khan intrusions). The second type is characterized by a cumulate and poikilitic texture and higher-Mg homogeneous olivine (the Zunduk and Ongureny intrusions). Cr-spinels in all intrusions have similar compositional features.

4. Petrography

In the inner part of the Moriany and Ulan-Khan intrusions, most of the rocks are porphyritic (Figure 2a,b) with phenocrysts of olivine (50–70 vol.%) and clinopyroxene (<10 vol.%) in a groundmass of olivine, clinopyroxene, minor phlogopite, opaque oxides, and apatite. In addition, there are samples with a poikilitic texture (Figure 2c,d). In most samples from both intrusions, serpentine partially or wholly replaces olivine (Figure 2a,b), while serpentine and chlorite replace groundmass minerals. Completely serpentinized olivine phenocrysts are euhedral (Figure 2a,b) and are up to 1 mm in size. Olivine in the matrix occur as smaller crystals. Relic olivine phenocrysts often have a zoned texture in both intrusions. Clinopyroxene and rare orthopyroxene occur as oikocrysts containing olivine chadacrysts (Figure 2c,d). Euhedral and subhedral Cr-spinel grains are enclosed in olivine as well as in the groundmass. Ilmenite occurs as anhedral interstitial grains between the groundmass silicates and forms intergrowths with Cr-rich magnetite and apatite and, very rarely, with rounded grains (up to 4–5 μm in diameter) of zircon (Figure 3). Samples from marginal parts of the intrusion are commonly completely serpentinized and/or chloritized.

The ultramafic rocks of the Zunduk and Ongureny intrusion show a cumulate and poikilitic texture and consist essentially of olivine (50–60%), clinopyroxene (20–30%), orthopyroxene (<10%), and accessory Cr-spinel (1–3%), along with a small amount of ilmenite and phlogopite. Also in these intrusions, there are rounded and subhedral zircon grains. Olivine grains are euhedral and up to 1.5 mm \times 2.5 mm in size (Figure 2e–h). Along with large crystals of olivine, rounded smaller grains (0.1–0.2 mm) are present, locally poikilitic and included in clinopyroxene (Figure 2h).

Clinopyroxenes occur commonly as oikocrysts containing olivine and, rarely, orthopyroxene chadacrysts. Euhedral and subhedral Cr-spinel grains are enclosed in olivine and in the interspaces. Alteration effects in the rocks of the Zunduk and Onguren intrusion are not widespread but occur as a serpentinization of olivine along cracks within and along grain boundaries. Sometimes, olivine grains are completely serpentinized (Figure 2f).

All intrusive rocks in this study contain sulfide minerals such as pentlandite, pyrrhotite, chalcopyrite, and cubanite. The size of sulfide aggregates reaches 0.5 cm. Magnetite often occurs along the borders of pyrrhotite grains. Platinum-group minerals (michenerite, frudite, sobolevskite, sperilite, platarsite, laurite) occur in the Ulan-Khan [22] and Zunduk [23] intrusions as small (up to 10 μm) numerous inclusions in sulfides, often on the boundaries of sulfide grains and the silicate matrix, and rarely in silicates.

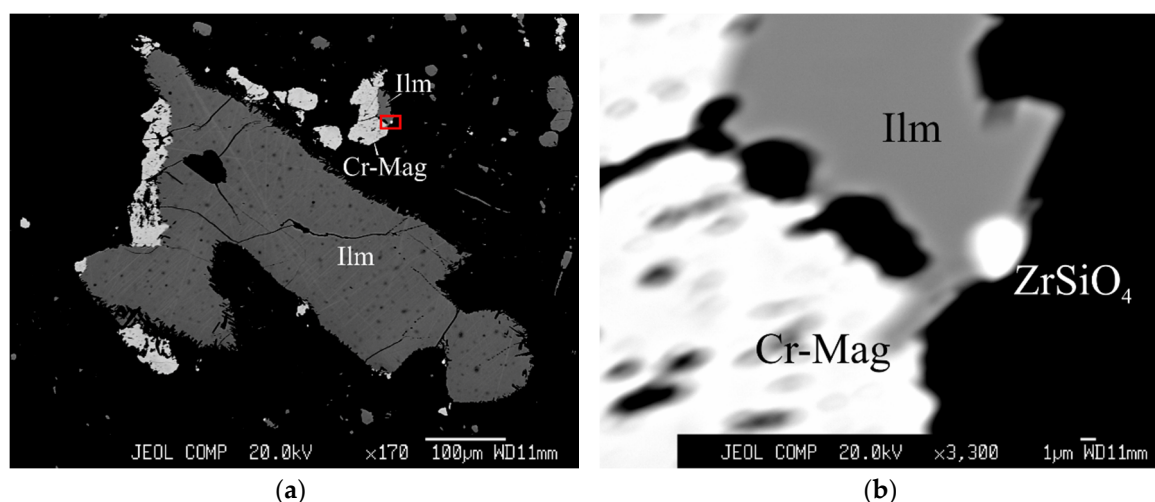


Figure 3. (a) Back-scattered electron image of ilmenite, Cr-rich magnetite, and zircon intergrowth (the Moriany intrusion). Sample 10143; (b) Enlarged fragment of Figure 3a (red rectangle). Ilm: ilmenite; Cr-Mag: Cr-rich magnetite; $ZrSiO_4$: zircon.

5. Results

5.1. Mineralogy

In the Moriany and Ulan-Khan intrusions, olivine phenocrysts have almost not been preserved. In both intrusions, there are zoned grains, which have MgO-rich cores (Fe_{79}) and FeO-rich rims (Fe_{70}). Groundmass olivine is characterized by low Fo (69–71 mol.%) in both intrusions. NiO exhibits minor compositional variation from 0.2 to 0.35 wt.% in olivine phenocrysts and ~0.2 wt.% in olivine of the groundmass. MnO content in olivine phenocrysts and groundmass differ and is 0.2–0.3 and 0.5–0.7 wt.%, respectively. Clinopyroxene is diopside with high Mg# (0.84–0.87) and has variable TiO_2 (0.2–0.7 wt.%) content and moderate Cr_2O_3 (0.9–1.0 wt.%) and Al_2O_3 (2.0–2.3 wt.%) content. Orthopyroxene is bronzite (Mg# = 0.80) with elevated Al_2O_3 (1.32 wt.%) and CaO (2.2 wt.%) and low TiO_2 (0.2 wt.%) and Cr_2O_3 (~0.4 wt.%). Ilmenite grains have slightly variable content of MgO (0.6–1.2 wt.%) and relatively constant MnO (2.0–2.3 wt.%). In the composition of apatite, F (0.8–1.0 wt.%) predominates over Cl (~0.3 wt.%).

Large olivine crystals from the Zunduk intrusion show a wide range of forsterite content (85–75 mol.%). Some grains are zoned, with Fo content ranging from 85 to 81 mol.% from core to rim. NiO content shows minor compositional variation (0.2–0.3 wt.%), but MnO content varies from 0.2 to 0.5 wt.%. Large olivine crystals from the Onguren intrusion have a narrow range of forsterite (Fe_{84-83}) and MnO (0.19–0.23 wt.%). NiO content varies from 0.2 to 0.3 wt.%. Core-rim zonation is not evident. Small olivine grains are characterized by lower Fe_{71-69} and NiO content (~0.2 wt.%) but higher MnO content (0.5–0.6 wt.%). Pyroxenes in both intrusions have similar compositions. Orthopyroxene is bronzite (Mg# = 0.80–0.84) with elevated Al_2O_3 (1.2 wt.%) and low TiO_2 (0.5 wt.%) and Cr_2O_3 (0.4 wt.%). Clinopyroxene is Cr-diopside and augite with high Mg# (0.85–0.88) and has a high TiO_2 (0.5–1 wt.%), Cr_2O_3 (0.7–1.3 wt.%), and Al_2O_3 (2.5 wt.%) content. Compositions of ilmenite from the Onguren intrusion are similar to those of the Moriany and Ulan-Khan intrusions.

5.2. Bulk-Rock Geochemistry

Major and trace element abundances of ultramafic rocks from the Primorsky Ridge are given in Tables S1 and S2. Some features of rock geochemistry are shown in Figure 4a–d. Ultramafic rocks have variable loss-on-ignition values (2.1–11 wt.%) and are characterized by relatively low SiO_2 (42–46 wt.%), CaO (2–6 wt.%), and total alkalis ($Na_2O + K_2O < 1$ wt.%); moderately low TiO_2 (0.2–0.5 wt.%); and high

MgO (26–36 wt.%) and FeO (9–13 wt.%). The content of Ni and Cr varies in wide ranges (800–1600 and 200–10,000 ppm, respectively). The rocks are characterized by variable but high $\text{Al}_2\text{O}_3/\text{TiO}_2$ (17–35).

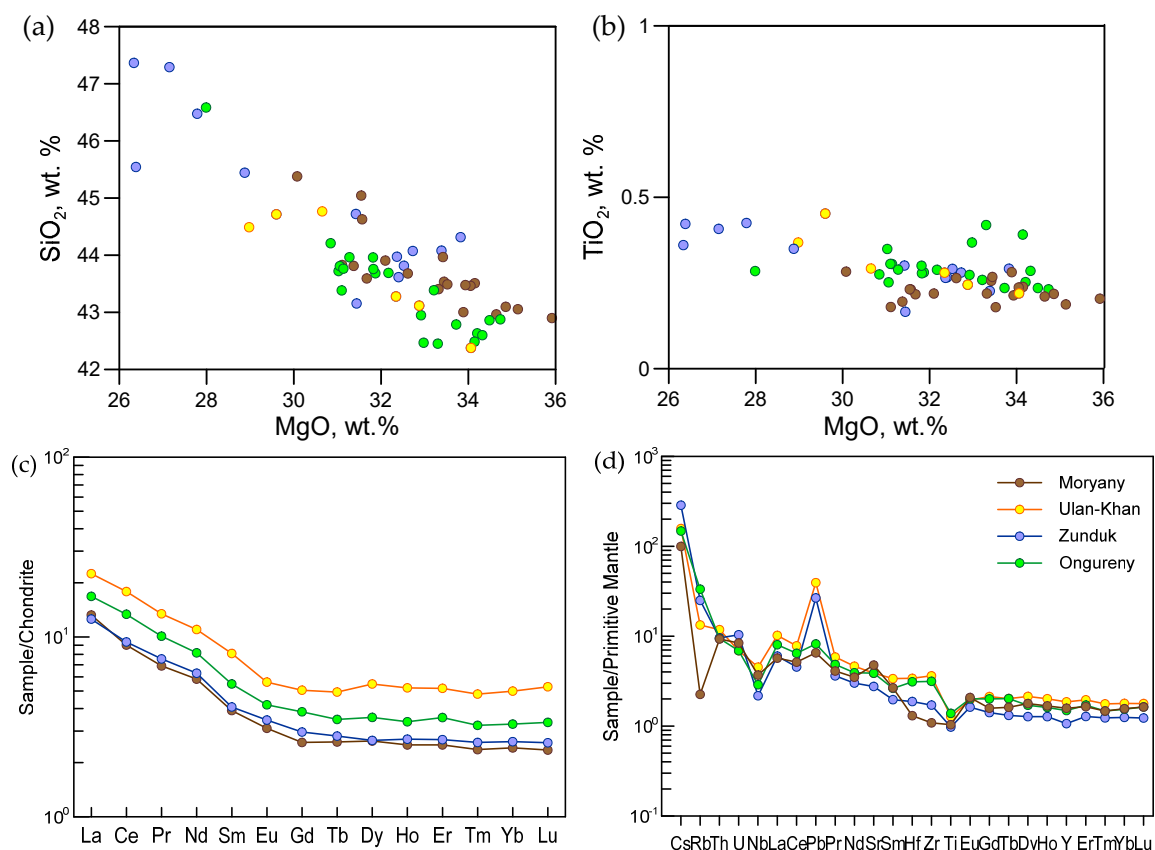


Figure 4. (a) SiO₂ and (b) MgO vs. TiO₂ plots. The major-element oxides were recalculated to 100% on a volatile-free base; (c) Chondrite-normalized [32] rare earth element (REE) and (d) Primitive Mantle-normalized [33] trace element abundance patterns for ultramafic rocks of the Primorsky Ridge.

The ultramafic intrusion from the Primorsky Ridge have a total rare earth element (REE) content of 17–42 ppm and exhibit identical chondrite-normalized light-REE-enriched patterns and relatively mid-REE (Figure 4c), with $\text{La}_N = 13\text{--}30$, $(\text{La}/\text{Sm})_N = 3.4\text{--}2.8$. Herewith, mid- and heavy-REEs show flat patterns with $(\text{Gd}/\text{Yb})_N$ around 1. In a primitive-mantle-normalized spidergram, they show patterns characterized by prominent Nb depletions with $(\text{Nb}/\text{La})_{\text{PM}}$ and $\text{Nb}/\text{Th}_{\text{PM}} < 1$, negative Ti ($\text{Ti}/\text{Gd}_{\text{PM}} = 0.59\text{--}0.72$), and generally positive Pb anomalies.

5.3. Cr-Spinel Chemistry

Two types of Cr-spinel were identified in ultramafic rocks from all intrusions. Type I Cr-spinel (Spl1) is enclosed in the inner part of olivine phenocrysts in the Moryany and Ulan-Khan intrusions and in large olivine crystals in the Zunduk and Ongureny intrusions (Figure 5c,e,g). They range in size from 20 to 30 μm and form equant crystals with cubic or modified octahedral shapes. Type II Cr-spinel (Spl2) occurs in the interstitial space, varies in size from 5 to 80 μm , and often has a zoned texture and a euhedral or irregular shape (Figure 5a,b,d,f,h). This type of Cr-spinel commonly occurs as an aggregate of small crystals or as individual grains. Representative microprobe analyses of Cr-spinels are given in Tables S3–S6. Compositional variations of Cr-spinels are shown in Figures 6, S5 and S6.

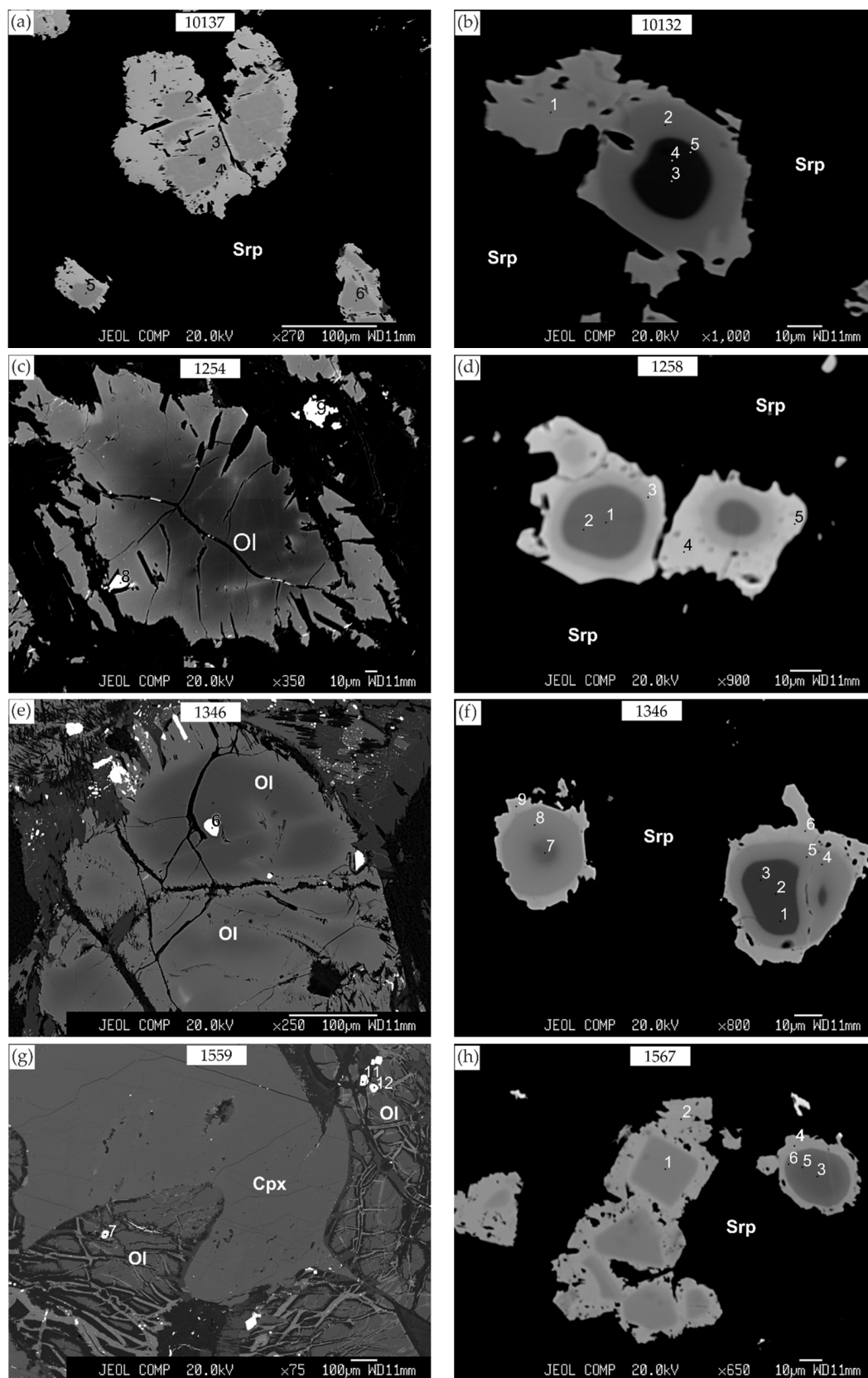


Figure 5. Back-scattered electron image of Cr-spinel from: (a,b) the Moryany intrusion; (c,d) The Ulan-Khan intrusion; (e,f) The Zunduk intrusion; (g,h) The Onguren intrusion. Ol: olivine; Cpx: clinopyroxene; Srp: serpentine. The points correspond to the analyses shown in Tables S3–S6.

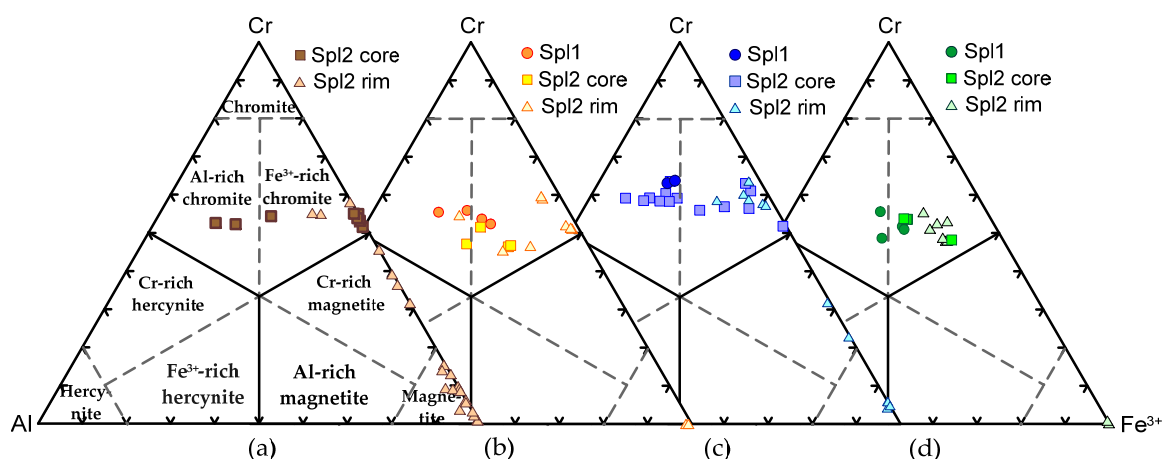


Figure 6. Compositional variations of Cr-spinels from ultramafic rocks of the Primorsky Ridge in terms of the Al-Cr-Fe³⁺ diagram. (a) The Moriany intrusion; (b) The Ulan-Khan intrusion; (c) The Zunduk intrusion; (d) The Ongureny intrusion. The diagrams are split to avoid overcrowding. The fields of spinel composition are from [34]. Spl1: Type I Cr-spinel; Spl2: Type II Cr-spinel.

5.3.1. The Moriany Intrusion

Data on the composition of Spl1 in the Moriany intrusion is not available. There are only data on Spl2, which occurs as homogeneous and zoned grains (Figure 5b). Most homogeneous Cr-spinels are Fe³⁺-rich chromites (Fe₂O₃ > FeO) with a high TiO₂ (1.7–2.5 wt.%) and MnO (1.3–1.5 wt.%) content, and with very low content of MgO and Al₂O₃ (≤0.7 and 0.1–0.2 wt.%, respectively). Sometimes, magnetite rims occur around Fe³⁺-rich chromite grains (Figure 5a). Magnetite rims have a low TiO₂ (0.4 wt.%) and Cr₂O₃ (0.5 wt.%) content.

Cr-spinels with a zoned texture have Al-rich chromite and Fe²⁺-rich chromite (FeO > Fe₂O₃) cores (Figure 6a), which are characterized by a higher content of Cr₂O₃, Al₂O₃, and MgO than homogeneous grains. In the zoned grains with Al-rich chromite cores, the content of Al₂O₃ and MgO decreases from core to rim (from 15.7 and 2.6 wt.% to 3.6 and 1.2 wt.%, respectively). This is coupled with an increase in TiO₂, MnO, and Fe₂O₃ content (Figure S6). Cr₂O₃ content varies in the narrow range (36.8–34.7 wt.%).

Cr-rich magnetite from intergrowths with ilmenite has a high TiO₂ (0.4–1.8 wt.%) and Cr₂O₃ (3.7–8.9 wt.%) content and a low MgO (0.4–0.7 wt.%) content.

5.3.2. The Ulan-Khan Intrusion

Spl1 in the Ulan-Khan intrusion is homogeneous and its composition corresponds to Al-chromite and Fe²⁺-rich chromite (Figure 6b) with a variable Al₂O₃ (8.1–13.7 wt.%) and Cr₂O₃ (32.1–36.8 wt.%) content, a low MgO (1.0–1.5 wt.%) content, and a moderately high TiO₂ (0.8–1.1 wt.%) content. It is characterized by relatively high Cr# (0.63–0.72 wt.%) and low Fe³⁺# (0.25–0.35) (Figures S5 and S6).

Spl2, such as that found in the Moriany intrusion, occurs both as homogeneous and zoned grains, with homogeneous grains displaying a lower TiO₂ (1.0–1.2 wt.%) and MnO (0.3–0.4 wt.%) content and higher MgO and Al₂O₃ (~1.0 and 6.0–8.0 wt.%, respectively) content.

Spl2 with a zoned texture has very contrasting cores and rims in the reflected light and on the back-scattered electron image. Occasionally, the concentric zonation shows several zones from the core to the rim (Figure 5d). There are grains with Al-rich chromite and Fe²⁺-rich chromite cores (FeO > Fe₂O₃), which are rimmed by Fe³⁺-rich chromite (Fe₂O₃ > FeO). The Al-rich chromite and Fe²⁺-rich chromite cores have a similar composition to that of the Moriany intrusion. Zoned grains are characterized by a decrease in the content of Cr₂O₃, Al₂O₃, and MgO from the core to the rim, which is commonly accompanied by an increase in the content of FeO and TiO₂.

5.3.3. The Zunduk Intrusion

Spl1 in the Zunduk intrusion is also homogeneous and shows lower Al₂O₃ (9.2–10.1 wt.%) content and higher MgO (2.5–3.0 wt.%), Cr₂O₃ (38.2–42.6 wt.%), and TiO₂ (1.5–1.8 wt.%) content than Spl1 of the Ulan-Khan intrusion. It is Al-chromite in composition (Figures 5e and 6c) and is characterized by low Mg# (0.16–0.18) and moderately high Cr# (0.7–0.76) (Figure S5).

Spl2 occurs as zoned grains. Such grains usually show a dark core and light rims, just as in other intrusions. There are grains with Al-rich chromite and Fe²⁺-rich chromite cores (FeO > Fe₂O₃) and Cr-rich magnetite cores (Figures 5f and 6c), which are rimmed by Fe³⁺-rich chromite (Fe₂O₃ > FeO), Cr-rich magnetite, and magnetite, respectively. In all zoned grains, TiO₂ and MnO content increases from core to rim.

The composition of the Al-rich chromite core of Spl2 is very similar to that of Spl1 but is characterized by lower Mg# (0.1–0.14), moderately high Cr# (0.64–0.7), and higher Al₂O₃ (10.6–14.3 wt.%). Fe²⁺-rich chromite cores show high TiO₂ (1.5–1.8 wt.%) and MnO (0.83 wt.%) content.

Magnetite in the outer rims of some Cr-spinels shows very limited compositional variability.

5.3.4. The Ongureny Intrusion

Like those in the Zunduk and Ulan-Khan intrusions, Cr-spinels in the Ongureny intrusion that are enclosed in olivine are homogeneous, but unlike them they have lower Cr₂O₃ (33.5–39.6 wt.%) and higher MgO (3.3–7.8 wt.%). They are Al-rich and Fe²⁺-rich chromites (Figures 5g and 6d) and are characterized by variable content of TiO₂ (1.0–5.3 wt.%), moderately high Cr# (0.7–0.83), and low Fe³⁺# (0.20–0.34).

Spl2 occurs as zoned grains. Zoned grains show a dark core and light rims, just as in other intrusions. There are grains with Fe²⁺-rich chromite (FeO > Fe₂O₃) and Fe³⁺-rich chromite cores (Fe₂O₃ > FeO) (for example, Figure 5h), which are rimmed by Cr-rich magnetite and magnetite, respectively.

Fe²⁺-rich chromite cores have a relatively high MgO (3.8–6.2 wt.%), Al₂O₃ (8–9 wt.%), and TiO₂ (2.6–2.8 wt.%) content, a low MnO (0.34–0.52 wt.%) content and low Fe³⁺# (0.25–0.27) ratio. Cr-rich magnetite cores are characterized by high TiO₂ (up to 5 wt.%) and moderately low Al₂O₃ (4.6 wt.%).

Magnetite occurring as an outer rim around Cr-spinels, such as in the Moriany intrusion, has a low TiO₂ (0.2–0.4 wt.%) and Cr₂O₃ (0.13–0.5 wt.%) content.

6. Discussion

6.1. Cr-Spinel Composition Variation and Zonation

6.1.1. Primary Composition

Cr-spinel is highly sensitive to modification during early hydrothermal alteration and following prograde metamorphism of host rocks [7,11,15,35–37]. There are two main features that are not typical of primary spinels [11]: (1) values of Mg/(Mg + Fe²⁺) < 0.15 and (2) an anomalously high Mn content. Unaltered Cr-spinels show a strong linear negative correlation between MnO and Mg/(Mg + Fe²⁺) [11]. Most Cr-spinels in ultramafic rocks of the Primorsky Ridge are characterized by very low Mg# and variable MnO (0.4–1.8 wt.%) content (Figures 7 and S7). A linear negative correlation between MnO and Mg/(Mg + Fe²⁺) within a 'Filter polygon' [11] occurs only in some Spl1 and Spl2 grains of the Onguren and Zunduk intrusions (Figure 7). Their compositions will be treated below as the magmatic Cr-spinel.

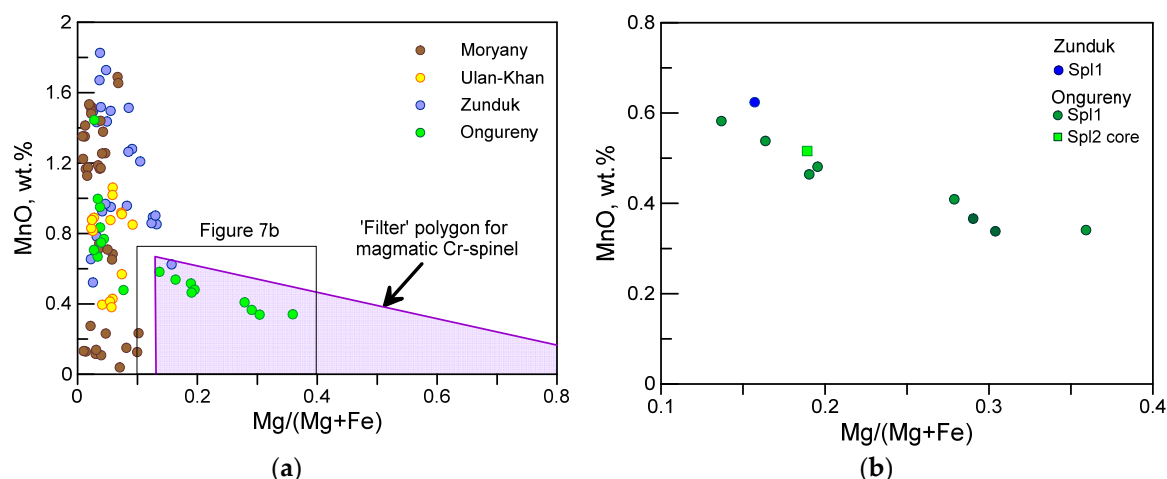


Figure 7. Mg/(Mg + Fe²⁺) vs. MnO (wt.%) diagram. (a) The entire Cr-spinel data set; (b) Selected analyses that fall into the 'Filter' polygon [11].

Magmatic Cr-spinels, represented by Al-rich chromite, occur mainly as inclusions in olivine and, rarely, in cores of zoned grains from the groundmass and the silicate interspaces. We assume that they crystallized earlier than the olivine crystals. Cr-spinels captured by olivine were not altered by reaction with interstitial evolving liquid, but the subsolidus Fe-Mg exchange between spinel and olivine can have a significant effect on the Cr-spinel composition [3,13,38]. With a decrease in temperature, spinel should be Fe-enriched due to the exchange equilibrium. The final Mg/(Mg + Fe²⁺) value of Cr-spinel grains depends on the composition of the co-existing olivine and the effective final equilibrium temperature, or blocking temperature, which is itself a function of the cooling mode [38,39]. Therefore, due to the low values of Mg/(Mg + Fe²⁺), some Cr-spinel grains enclosed in olivine could be considered to be the result of such a subsolidus exchange.

The Cr-spinel from groundmass may have reacted directly with interstitial liquid, and its composition could change significantly, including a substantial decrease in the Mg, Cr, and Al content and an increase in the Fe²⁺ and Ti content. This evolution of spinel composition was observed in the Jinchuan [40,41], Pechenga [42], and Noril'sk [43,44] intrusions.

In our opinion, the homogeneous Fe²⁺-rich chromite and zoned Cr-spinel grains with the Fe²⁺-rich chromite cores crystallized after the Al-rich chromite. The higher Ti and Fe²⁺, as well as the lower Cr content in these grains, characterize this spinel as a late phase that crystallized from a more evolved and fractionated melt (Figure 5b,d,f (4 and 5 points)).

A specific feature of Cr-spinels in the ultramafic rocks of the Primorsky Ridge is their noticeably high TiO₂ content (up to 6.5 wt.%) (Figure 8). The presence of a high TiO₂ content in Cr-spinels enclosed in olivine crystals may be a clear indication of the primary magmatic nature of Ti enrichment. Previously, it was shown [13,38] that Cr-spinels could easily exchange Mg and Fe²⁺ by interdiffusion through olivine grains, but that Cr-spinels enclosed in early crystallizing olivine were protected from Ti enrichment owing to the difficulty of diffusing Ti through the olivine structure. Ti could exchange, but at a much slower rate. An increase in the TiO₂ content should be accompanied by an increase in Fe₂O₃ content, which is not typical for studied Cr-spinels enclosed in olivine.

Ti-rich Cr-spinels have been recorded in many mafic-ultramafic igneous complexes, such as the Jinchuan layered intrusion [38,39], gabbro-wehrlite intrusions of the Pechenga area [42], Noril'sk-Talnakh intrusions [43,44], meimechites [45,46], intrusions of the Karoo province [47–49], Mg-rich rocks of the Deccan Traps [50], picrites of Hawaii [51], ferropicritic rocks from the Mino-Tamba belt (SW Japan) [52,53], and Snake River Plain volcanics [54].

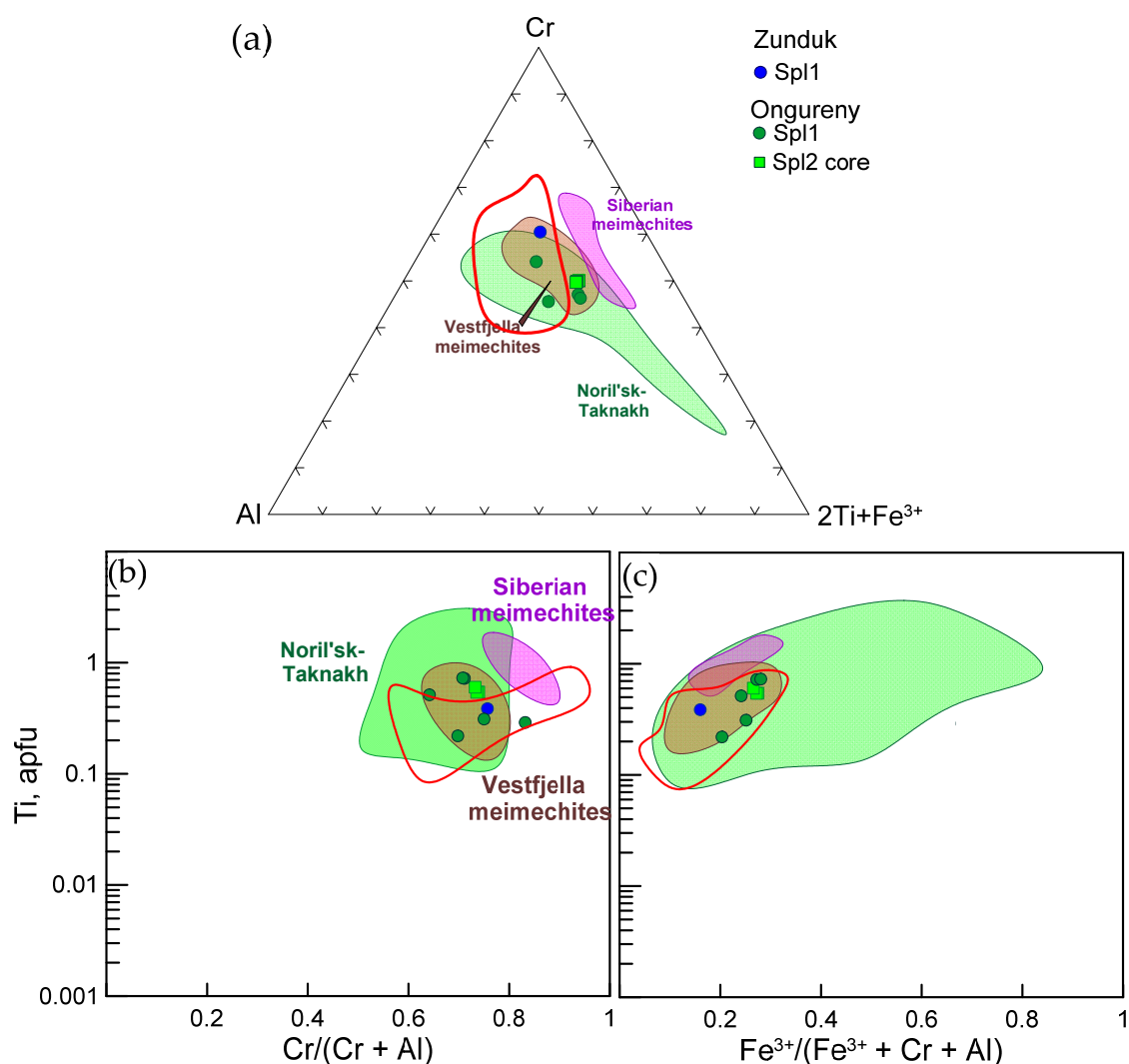


Figure 8. Compositional variations of primary Cr-spinels from ultramafic rocks of the Primorsky Ridge: (a) the Al-Cr-2Ti + Fe³⁺; (b) Cr/(Cr + Al), and (c) Fe³⁺/(Fe³⁺ + Cr + Al) vs. Ti (apfu on the basis of 32 oxygen anions) diagrams. The field of spinel compositions: Vestfjella meimechites [45], Siberian meimechites [46], Noril'sk-Talnakh intrusions [43], and Neoproterozoic mafic-ultramafic intrusions (Tartay and Medek) (red contour) [55] are plotted for comparison.

Based on the assumption that the emplacement of the high-Mg intrusion of the Primorsky Ridge took place in an intracontinental setting, the closest analogues for studied Cr-spinels may be Cr-spinels from Siberian and Karoo meimechites and Noril'sk-Talnakh intrusions. Cr-spinel from Siberian meimechites [46] are characterized by higher TiO₂ and MgO content and lower Al₂O₃ content (Figure 8). Primary composition of the studied Cr-spinels is close to the compositional trend shown by Vestfjella meimechites of the Karoo Large Igneous province [45] and the Noril'sk-Talnakh intrusion [43] (Figure 8).

Compared with Cr-spinels from other Neoproterozoic mafic-ultramafic intrusions of southern Siberia [55,56], the studied spinels are characterized by lower Al₂O₃ and MgO content and higher Cr₂O₃, TiO₂, and FeO content. However, the elevated content of TiO₂ (up to 2 wt.%) was previously detected in spinels from silicate interspaces of the Tartai and Medek intrusions [56]. Interestingly, melt inclusions characterized by a high content of TiO₂, FeO, and P were found in these Cr-spinels [56]. The field of the compositions of these Cr-spinels partially overlaps with that of the studied Cr-spinels (Figure 8).

6.1.2. Alteration of Cr-Spinel

As mentioned above, the primary igneous composition of Cr spinels and host rocks is usually modified by serpentinization and regional metamorphism [7,11,15,35–37]. The studied rocks mostly show only alterations as a result of serpentinization. The secondary alteration of Cr-spinel usually results in a highly reflective border along the grain rims. During serpentinization, the Cr-spinel can also incorporate Mn from hydrothermal fluids [15,36] (Figure 7). Fe³⁺-rich, Mg-Al depleted rims can be formed by a reaction between the primary Cr-spinel and secondary magnetite deposited on the Cr-spinel grains during serpentinization [15,36,57] or by dissolution of the primary chromite with later re-precipitation into Fe²⁺-rich chromite under hydrothermal conditions [58–60]. Probably, in the grains with the primary Fe²⁺-rich chromite composition, the formation of Fe³⁺-rich chromite occurred according to the first model (Figure 5a). This assumption is supported by the low TiO₂ content of the magnetite rims, which cannot be related to the local mobility of Ti [42]. In grains with an Al-rich chromite core, serpentinization led to the formation of Cr-rich magnetite rims (Figure 5f (6 and 9 points)).

6.2. Petrogenetic Consequences

It is generally recognized that the diffusion capacity of Ti⁴⁺ in olivine is relatively low [5,9,13]; therefore, the content of TiO₂ in Cr-spinel can be a trustworthy indicator of the magma composition. In addition, abundant data suggest that the TiO₂ content in Cr-spinel increases from island arc to intraplate magmas [5,9,61]. This indicates the potential suitability of TiO₂ content in Cr-spinel for tectonic discrimination of Mg-rich igneous assemblages.

The dependence of spinel Al₂O₃ and TiO₂ contents on the parental melt composition suggests that the Al/Ti ratio can be successfully used to distinguish between different magma types, their tectonic affinities, and mantle sources [6]. The composition of magmatic Cr-spinels of ultramafic rocks of the Primorsky Ridge lies within, or close to, the ocean island basalts (OIB) and LIP compositional fields in the discrimination diagram by Kamenetsky et al. [6] (Figure 9).

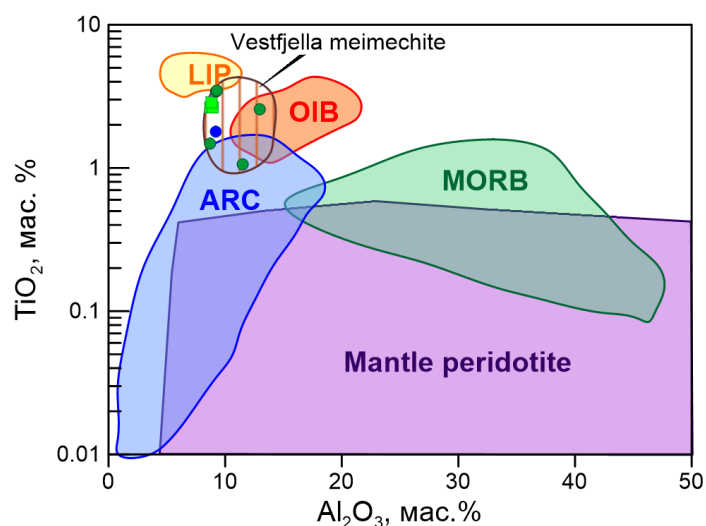


Figure 9. Al₂O₃ vs. TiO₂ for primary Cr-spinels of the Ulan-Khan and Onguren intrusions. Fields LIP, OIB, ARC, MORB, mantle peridotite after [6], and Vestfjella meimechites after [45]. LIP: large igneous provinces; OIB: oceanic island basalts; ARC: island arcs; MORB: mid-ocean ridge basalts.

As mentioned above, the ultramafic rocks of the Primorsky Ridge are low in SiO₂, TiO₂, K₂O, and Na₂O and very high in MgO. SiO₂ and TiO₂ (Figure 4a,b) increase with decreasing MgO, which suggests that the compositional trend was mainly controlled by olivine accumulation. In the Pearce molecular ratio diagram (Figure S8a), all samples follow a coherent compositional trend. The slope

of this trend (1.97) is close to the ideal index of 2.0 for crystal addition/separation of olivine [62–64]. The MgO/Al₂O₃ vs. FeO/Al₂O₃ plot (Figure S8) indicates that all samples fall on a single trend. The slope of this trend indicates that the MgO/FeO mole ratio of the fractionating ferromagnesian phase had an average value of 12.21. Assuming that all iron was in the ferrous state, this is equivalent to fractionation of olivine with an average composition of Fo ~89. If 10% of the total iron in the melt was in the ferric state, the olivine composition would be Fo ~90. The FeO/MgO ratio of the parental melt, estimated using the equation of Roeder and Emslie [65], is ~0.4. The olivine and Cr-spinel in ultramafic rocks of the Ongureny intrusion are less affected by post magmatic alteration and most likely represent the early crystallization phases from the parental melt. The Al₂O₃ and TiO₂ content of the parental melt in equilibrium with Cr-spinel can be calculated using an experimentally determined formula with the assumption that Al₂O₃ and TiO₂ content in spinel is the only function of Al₂O₃ and TiO₂ content in the melt [6,66]. The calculated Al₂O₃ and TiO₂ content of the parental melt are 11.15–11.89 and 1.14–1.66 wt.%, respectively.

Previously, it was found that, in southern Siberia, there is the Neoproterozoic (ca 720 Ma) Irkutsk Large Igneous Province [21], which consist of Ni-Cu-PGE ore-bearing dunite-peridotite-pyroxenite-gabbro complexes (Tartai, Upper Kingash, Ioko-Dovyren intrusions), along with the Sayan and Baikal dolerite dykes [30,31]. They converge along the margin of the Irkutsk Promontory, which has led to the assumption that they are part of a radiating magmatic swarm [21]. The high-Mg intrusions of the Primorsky Ridge, intersecting metamorphic rocks of the Sarma Group and granitoids of the Paleoproterozoic Primorsk complex, could be part of a single magmatic event with the above mentioned igneous complexes.

7. Conclusions

This study of the chemical composition of Cr-spinels in the ultramafic rocks of the Primorsky Ridge (Western Baikal region) have brought us to the following conclusions:

- (1) Two types of Cr-spinel were identified in ultramafic rocks from all intrusions. Type I Cr-spinel is enclosed in the inner part of olivine crystals and is homogeneous Al-rich chromite and Fe²⁺-rich chromite. Type II Cr-spinel occurs in the interstitial space as homogeneous and zoned grains with Al-rich chromite and Fe²⁺-rich chromite cores.
- (2) A specific feature of Cr-spinels in ultramafic rocks of the Primorsky Ridge is their noticeably high TiO₂ content (up to 6.5 wt.%).
- (3) Magmatic Cr-spinels, represented by Al-rich chromite, occur mainly as inclusions in olivine and, rarely, in cores of zoned grains. They crystallized earlier than the olivine crystals.
- (4) The homogeneous Fe²⁺-rich chromite and zoned Cr-spinel grains of type II crystallized after Al-rich chromite from a more evolved and fractionated melt.
- (5) Serpentinization led to the formation of Fe³⁺-rich chromite, Cr-rich magnetite, and magnetite rims.

The data on the compositional variation of Cr-spinel in high-Mg intrusions of the Primorsky Ridge (Western Baikal region, Russia) presented here could be considered as a starting point for further geochemical research.

Supplementary Materials: The following are available online at <http://www.mdpi.com/2075-163X/10/7/608/s1>. Figure S1: View of the Primorsky Ridge from Lake Baikal, Figure S2: (a) View of the Onguren intrusion from the Zunduk intrusion, (b) The outcrop of the Onguren intrusion ultramafic rocks, Figure S3: The outcrop of the Ulan-Khan intrusion, Figure S4: Large blocks of eluvium, the Moriany intrusion, Figure S5: Cr/(Fe³⁺ + Cr + Al) vs. Ti (apfu on the basis of 32 oxygen anions) diagram. The diagrams are split to avoid overcrowding. Sp1: Type I Cr-spinel; Sp2: Type II Cr-spinel, Figure S6: Fe³⁺/(Fe³⁺ + Cr + Al) vs. Ti (apfu on the basis of 32 oxygen anions) diagram. The diagrams are split to avoid overcrowding. Sp1: Type I Cr-spinel; Sp2: Type II Cr-spinel, Figure S7: Mg/(Mg + Fe²⁺) vs. MnO (wt.%) diagram. The diagrams are split to avoid overcrowding. Sp1: Type I Cr-spinel; Sp2: Type II Cr-spinel, Figure S8: Molecular proportion ratio plot of the Ongureny intrusion rocks. Vectors whose slopes are consistent with the fractionation of olivine (Ol) and clinopyroxene (Cpx) are shown in panel (a). Table S1: Bulk-rock major elements (wt.%), Cr and Ni (ppm) content of ultramafic rocks from the Primorsky Ridge (Western Baikal region), Table S2: Trace-element (ppm) composition of ultramafic rock from the Primorsky Ridge (Western Baikal region), Table S3: Representative electron microanalyses of Cr-spinel and magnetite (wt.%) from

ultramafic rocks of the Moryany intrusion, Table S4: Representative electron microanalyses of Cr-spinel (wt.%) from ultramafic rocks of the Ulan-Khan intrusion, Table S5: Representative electron microanalyses of Cr-spinel and Cr-rich magnetite (wt.%) from ultramafic rocks of the Zunduk intrusion, Table S6: Representative electron microanalyses of Cr-spinel and magnetite (wt.%) from ultramafic rocks of the Onguren intrusion.

Author Contributions: Methodology, investigation, project administration, and writing—original draft preparation, A.S.M.; investigation and writing—original draft preparation, T.B.K.; investigation and resources, A.A.D.; investigation and resources, E.E.P. All authors have read and agreed to the published version of the manuscript.

Funding: The research was performed within the frame of the state order project IX.129.1, No. 0350-2019-0008.

Acknowledgments: The authors highly appreciate the great efforts of three anonymous reviewers, whose recommendations greatly improved the presentation of the research results. We are also grateful to Yu.P. Beneduk and M.Yu. Podlipskii for their assistance in field works.

Conflicts of Interest: The authors declare no conflict of interest.

References

1. MacGregor, I.D.; Smith, C.H. The use of chrome spinels in petrographic studies of ultramafic intrusions. *Can. Mineral.* **1963**, *7*, 403–412.
2. Irvine, T.N. Chromian spinel as a petrogenetic indicator: Part I. Theory. *Can. J. Earth Sci.* **1965**, *2*, 648–672. [[CrossRef](#)]
3. Irvine, T.N. Chromian spinel as a petrogenetic indicator: Part II. Petrologic applications. *Can. J. Earth Sci.* **1967**, *4*, 71–103. [[CrossRef](#)]
4. Dick, H.J.B.; Bullen, T. Chromian spinel as a petrogenetic indicator in abyssal and Alpine-type peridotites and spatially associated lavas. *Contrib. Mineral. Petrol.* **1984**, *86*, 54–76. [[CrossRef](#)]
5. Arai, S. Chemistry of chromian spinel in volcanic rocks a potential guide to magma chemistry. *Mineral. Mag.* **1992**, *56*, 173–184. [[CrossRef](#)]
6. Kamenetsky, V.S.; Crawford, A.J.; Meffre, S. Factors controlling chemistry of magmatic spinel: An empirical study of associated olivine, Cr-spinel and melt inclusions from primitive rocks. *J. Petrol.* **2001**, *42*, 655–671. [[CrossRef](#)]
7. Barnes, S.J.; Roeder, P.L. The range of spinel compositions in terrestrial mafic and ultramafic rocks. *J. Petrol.* **2001**, *42*, 2279–2302. [[CrossRef](#)]
8. Dare, S.A.; Pearce, J.A.; McDonald, I.; Styles, M.T. Tectonic discrimination of peridotites using f_{O_2} -Cr# and Ga-Ti-Fe III systematics in chrome-spinel. *Chem. Geol.* **2009**, *261*, 199–216.
9. Arai, S.; Okamura, H.; Kadoshima, K.; Tanaka, C.; Suzuki, K.; Ishimaru, S. Chemical characteristics of chromian spinel in plutonic rocks: Implications for deep magma processes and discrimination of tectonic setting. *Island Arc* **2011**, *20*, 125–137. [[CrossRef](#)]
10. Barnes, S.J. Chromite in komatiites, I. Magmatic controls on crystallization and composition. *J. Petrol.* **1998**, *39*, 1689–1720. [[CrossRef](#)]
11. Evans, B.W.; Frost, B.R. Chrome-spinel in progressive metamorphism—A preliminary analysis. *Geochim. Cosmochim. Acta* **1975**, *39*, 959–972. [[CrossRef](#)]
12. Cameron, E.N. Postcumulus and subsolidus equilibration of chromite and coexisting silicates in the Eastern Bushveld Complex. *Geochim. Cosmochim. Acta* **1975**, *39*, 1021–1033. [[CrossRef](#)]
13. Scowen, P.A.H.; Roeder, P.L.; Helz, R.T. Re-equilibration of chromite within Kilauea Iki lake, Hawaii. *Contrib. Mineral. Petrol.* **1991**, *107*, 8–20. [[CrossRef](#)]
14. Peltonen, P. Crystallization and re-equilibration of zoned chromite in ultramafic cumulates, Vammala Ni-belt, southwestern Finland. *Can. Mineral.* **1995**, *33*, 521–535.
15. Barnes, S.J. Chromite in Komatiites II. Modification during greenschist to mid amphibolite facies metamorphism. *J. Petrol.* **2000**, *41*, 387–409. [[CrossRef](#)]
16. Sakuyama, M. Evidence of magma mixing: Petrological study of Shiroumaoike calc-alkaline andesite volcano, Japan. *J. Volcanol. Geotherm. Res.* **1978**, *5*, 179–208. [[CrossRef](#)]
17. Fisk, M.R.; Bence, A.E. Experimental crystallization of chrome spinel in famous basalt. *Earth Planet. Sci. Lett.* **1980**, *48*, 111–123. [[CrossRef](#)]
18. Sobolev, N.V.; Logvinova, A.M. Significance of accessory chrome spinel in identifying serpentinite paragenesis. *Int. Geol. Rev.* **2005**, *47*, 58–64. [[CrossRef](#)]

19. Mekhonoshin, A.S.; Ernst, R.; Söderlund, U.; Hamilton, M.A.; Kolotilina, T.B.; Izokh, A.E.; Polyakov, G.V.; Tolstykh, N.D. Relationship between platinum-bearing ultramafic-mafic intrusions and large igneous provinces (exemplified by the Siberian Craton). *Russ. Geol. Geophys.* **2016**, *57*, 822–833. [[CrossRef](#)]
20. Ariskin, A.A.; Kostitsyn, Y.A.; Konnikov, E.G.; Danyushevsky, L.V.; Meffre, S.; Nikolaev, G.S.; McNeill, A.; Kislov, E.V.; Orsoev, D.A. Geochronology of the Dovyren intrusive complex, northwestern Baikal area, Russia, in the Neoproterozoic. *Geochem. Inter.* **2013**, *51*, 859–875. [[CrossRef](#)]
21. Ernst, R.E.; Hamilton, M.A.; Söderlund, U.; Hanes, J.A.; Gladkochub, D.P.; Okrugin, A.V.; Kolotilina, T.B.; Mekhonoshin, A.S.; Bleeker, W.; LeCheminant, A.N.; et al. Long-lived connection between southern Siberia and northern Laurentia in the Proterozoic. *Nat. Geosci.* **2016**, *9*, 464–472. [[CrossRef](#)]
22. Mekhonoshin, A.S.; Podlipskii, M.Y.; Doroshkov, A.A.; Kolotilina, T.B. Picrite magmatism of the Western Baikal region. In *Geodynamic Evolution of the Lithosphere in the Central Asian Mobile Belt: From Ocean to Continent*; IEC SB RAS: Irkutsk, Russia, 2015. (In Russian)
23. Tolstykh, N.D.; Podlipskii, M.Y.; Mekhonoshin, A.S.; Kolotilina, T.B.; Polyakov, G.V. Ulan Khan and Zunduk massifs (Western Baikal Region) as part of the East Siberian metallogenic province. In Proceedings of the Science Meeting, Tomsk, Russia, 27–30 November 2018. (In Russian).
24. Lavrent'ev, Y.G. High current electron probe microanalysis of minerals. *X-ray Spectrom.* **2010**, *39*, 37–40.
25. Lavrent'ev, Y.G. New Trends in X-Ray Microanalysis of Minerals (Review). *Inorg. Mater.* **2010**, *46*, 1605–1612. [[CrossRef](#)]
26. Rosen, O.M.; Condie, K.C.; Natapov, L.M.; Nozhkin, A.D. Archean and Early Proterozoic evolution of the Siberian Craton: A preliminary assessment. In *Archean Crustal Evolution*; Condie, K.C., Ed.; Elsevier: Amsterdam, The Netherlands, 1994; pp. 411–459. ISBN1 0444816216. ISBN2 978-0444816214.
27. Gladkochub, D.; Pisarevsky, S.; Donskaya, T.; Natapov, L.M.; Mazukabzov, A.; Stanevich, A.M.; Sklyarov, E. The Siberian Craton and its evolution in terms of Rodinia hypothesis. *Episodes* **2006**, *29*, 169–174. [[CrossRef](#)]
28. Donskaya, T.V.; Gladkochub, D.P.; Pisarevsky, S.A.; Poller, U.; Mazukabzov, A.M.; Bayanova, T.B. Discovery of Archean crust within the Akitkan orogenic belt of the Siberian craton: New insight into its architecture and history. *Precam. Res.* **2009**, *170*, 61–72. [[CrossRef](#)]
29. Donskaya, T.V.; Bibikova, E.V.; Mazukabzov, A.M.; Kozakov, I.K.; Gladkochub, D.P.; Kirnozova, T.I.; Plotkina, Y.V.; Reznitsky, L.Z. The Primorsky granitoid complex of Western Cisbaikalia: Geochronology and geodynamic typification. *Russ. Geol. Geoph.* **2003**, *44*, 1006–1016.
30. Gladkochub, D.P.; Pisarevsky, S.A.; Donskaya, T.V.; Ernst, R.E.; Wingate, M.T.D.; Söderlund, U.; Mazukabzov, A.M.; Sklyarov, E.V.; Hamilton, M.A.; Hanes, J.A. Proterozoic mafic magmatism in Siberian craton: An overview and implications for paleocontinental reconstruction. *Precambrian Res.* **2010**, *183*, 660–668. [[CrossRef](#)]
31. Gladkochub, D.P.; Donskaya, T.V.; Ernst, R.; Mazukabzov, A.M.; Sklyarov, E.V.; Pisarevsky, S.A.; Wingate, M.; Söderlund, U. Proterozoic basic magmatism of the Siberian Craton: Main stages and their geodynamic interpretation. *Geotectonics* **2012**, *46*, 273–284. [[CrossRef](#)]
32. Sun, S.; McDonough, W.F. Chemical and isotopic systematics of oceanic basalts: Implications for mantle composition and processes. *Geol. Soc. Spec. Publ.* **1989**, *42*, 313–345. [[CrossRef](#)]
33. McDonough, W.F.; Sun, S.-S. The composition of the Earth. *Chem. Geol.* **1995**, *120*, 223–253. [[CrossRef](#)]
34. Bosi, F.; Biagioni, C.; Pasero, M. Nomenclature and classification of the spinel supergroup. *Eur. J. Mineral.* **2019**, *31*, 183–192. [[CrossRef](#)]
35. Gervilla, F.; Padrón-Navarta, J.A.; Kerestedjian, T.; Sergeeva, I.; González-Jiménez, J.M.; Fanlo, I. Formation of ferrian chromite in podiform chromitites from the Golyamo Kamenyane serpentinite, Eastern Rhodopes, SE Bulgaria: A two-stage process. *Contrib. Mineral. Petrol.* **2012**, *164*, 643–657. [[CrossRef](#)]
36. Barra, F.; Gervilla, F.; Hernández, E.; Reich, M.; Padrón-Navarta, J.A.; González-Jiménez, J.M. Alteration patterns of chromian spinels from La Cabaña peridotite, south-central Chile. *Mineral. Petrol.* **2014**, *108*, 819–836. [[CrossRef](#)]
37. Ruan, B.; Yu, Y.; Lv, X.; Feng, J.; Wei, W.; Wu, C.; Wang, H. Occurrence and mineral chemistry of chromite and related silicates from the Hongshishan mafic-ultramafic complex, NW China with petrogenetic implications. *Mineral. Petrol.* **2017**, *111*, 693–708. [[CrossRef](#)]
38. Roeder, P.L.; Campbell, I.H.; Jamieson, H.E. Re-evaluation of the olivine-spinel geothermometer. *Contrib. Mineral. Petrol.* **1979**, *68*, 325–334. [[CrossRef](#)]

39. Sack, R.; Ghiorso, M.S. Chromian spinels as petrogenetic indicators: Thermodynamic and petrological applications. *Am. Mineral.* **1991**, *76*, 827–847.
40. Barnes, S.J.; Tang, Z.-L. Chrome spinels from the Jinchuan Ni–Cu sulfide deposit, Gansu Province, People’s Republic of China. *Econ. Geol.* **1999**, *94*, 343–356. [[CrossRef](#)]
41. Yang, X.Z.; Matsueda, H.; Ishihara, S. Mode of occurrence, chemical composition, and origin of Cr–Fe–Ti oxides of the Jinchuan Ni–Cu–PGE deposits, China. *Int. Geol. Rev.* **1994**, *36*, 311–327. [[CrossRef](#)]
42. Abzalov, M.Z. Chrome-spinel in gabbro-wehrlite intrusions of the Pechenga area, Kola Peninsula, Russia: Emphasis on the alteration features. *Lithos* **1998**, *43*, 109–134. [[CrossRef](#)]
43. Barnes, S.J.; Kuniylov, V.Y. Spinels and Mg-ilmenites from the Noril’sk 1 and Talnakh intrusions and other mafic rocks of the Siberian flood basalt province. *Econ. Geol.* **2000**, *95*, 1701–1717. [[CrossRef](#)]
44. Ryabov, V.; Gora, M.; Shevko, A.Y. *Trap Magmatism and Ore Formation in the Siberian Noril’sk Region*; Springer: Berlin/Heidelberg, Germany, 2014; p. 390. ISBN 978-94-007-5022-7.
45. Heinonen, J.S.; Luttinen, A.V. Mineral chemical evidence for extremely magnesian subalkaline melts from the Antarctic extension of the Karoo large igneous province. *Mineral. Petrol.* **2010**, *99*, 201–217. [[CrossRef](#)]
46. Vasil’ev, Y.R.; Gora, M.P.; Kuz’min, D.V. Petrology of foiditic and meymechitic volcanism in the Maimecha-Kotui province (Polar Siberia). *Russ. Geol. Geoph.* **2017**, *58*, 659–673.
47. Eales, H.V. Anomalous Karoo spinels along the chromite–titanomagnetite join. *S. Afr. J. Sci.* **1979**, *75*, 24–29.
48. Eales, H.V.; Snowden, D.V. Chromiferous spinels of the Elephant’s Head dike. *Econ. Geol.* **1979**, *14*, 227–242. [[CrossRef](#)]
49. Cawthorn, R.G.; de Wet, M.; Hatton, C.J.; Cassidy, K. Ti-rich chromite from Mount Ayliff intrusion, Transkei: Further evidence for high Ti tholeiitic magma. *Am. Mineral.* **1991**, *76*, 561–573.
50. Melluso, L.; De Gennaro, R.; Rocco, I. Compositional variations of chromiferous spinel in Mg-rich rocks of the Deccan Traps, India. *J. Earth Syst. Sci.* **2010**, *119*, 343–363. [[CrossRef](#)]
51. Wilkinson, J.F.G.; Hensel, H.D. The petrology of some picrites from Mauna Loa and Kilauea volcanoes, Hawaii. *Contrib. Mineral. Petrol.* **1988**, *98*, 326–345. [[CrossRef](#)]
52. Ichiyama, Y.; Ishiwatari, A.; Hirahara, Y.; Shuto, K. Geochemical and isotopic constraints on the genesis of the Permian ferropicritic rocks from the Mino-Tamba belt, SW Japan. *Lithos* **2006**, *89*, 47–65. [[CrossRef](#)]
53. Ichiyama, Y.; Ishiwatari, A.; Koizumi, K. Petrogenesis of greenstones from the Mino–Tamba belt, SW Japan: Evidence for an accreted Permian oceanic plateau. *Lithos* **2008**, *100*, 127–146. [[CrossRef](#)]
54. Thompson, R.N. Titanian chromite and chromian titanomagnetite from a Snake River Plain basalt, a terrestrial analogue of lunar spinels. *Am. Mineral.* **1973**, *58*, 826–830.
55. Bedyuk, Y.P.; Simonov, V.A.; Mekhonoshin, A.S.; Kolotilina, T.B.; Stupakov, S.I.; Doroshkov, A.A. Genesis of ultramafic rocks of the Alkhadyr terrane (East Sayan, Siberia): Implications from the data on Cr-spinel compositions. *Russ. Geol. Geoph.* **2015**, *56*, 1308–1321. [[CrossRef](#)]
56. Pushkarev, E.V.; Votyakov, S.L.; Chashchukhin, I.S.; Kislov, E.V. Olivine–chromspinel oxythermobarometry of ultramafic rocks of the Ioko–Dovyren layered massif. *Dokl. Earth Sci.* **2004**, *395*, 266–270.
57. Bliss, N.W.; MacLean, W.H. The paragenesis of zoned chromite from central Manitoba. *Geochim. Cosmochim. Acta* **1975**, *39*, 973–990. [[CrossRef](#)]
58. Burkhard, D.J.M. Accessory chromium spinels, their coexistence and alteration in serpentinites. *Geochim. Cosmochim. Acta* **1993**, *57*, 1297–1306. [[CrossRef](#)]
59. Mukherjee, R.; Mondal, S.K.; Rosing, M.T.; Frei, R. Compositional variations in the Mesoarchean chromitites of the Nuggihalli schist belt, Western Dharwar Craton (India): Potential parental melts and implications for tectonic setting. *Contrib. Miner. Petrol.* **2010**, *160*, 865–885. [[CrossRef](#)]
60. Wylie, A.N.; Candela, P.A.; Burke, T.M. Compositional zoning in unusual Zn-rich chromite from the Sykesville district of Maryland and its bearing on the origin of “ferritchromite”. *Am. Mineral.* **1987**, *72*, 413–422.
61. Glassley, W. Geochemistry and tectonics of the Crescent Volcanic Rocks, Olympic Peninsula, Washington. *Geol. Soc. Am. Bull.* **1974**, *85*, 785–794. [[CrossRef](#)]
62. Pearce, T.H. Olivine fractionation equations for basaltic and ultrabasic liquids. *Nature* **1978**, *276*, 771–774. [[CrossRef](#)]
63. Beswick, A.E. Primary fractionation and secondary alteration within an Archean ultramafic lava flow. *Contrib. Mineral. Petrol.* **1983**, *82*, 221–231. [[CrossRef](#)]
64. Pearce, T.H. The identification and assessment of spurious trends in Pearce-type ratio variation diagrams: A discussion of some statistical arguments. *Contrib. Mineral. Petrol.* **1987**, *97*, 529–534. [[CrossRef](#)]

65. Roeder, P.L.; Emslie, R. Olivine-liquid equilibrium. *Contrib. Mineral. Petrol.* **1970**, *29*, 275–289. [[CrossRef](#)]
66. Maurel, C.; Maurel, P. Étude expérimentale de la distribution de l'aluminium entre bain silicaté basique et spinelle chromifère. Implications pétrogénétiques: Teneur en chrome des spinelles. *Bull. Mineral.* **1982**, *105*, 197–202. [[CrossRef](#)]



© 2020 by the authors. Licensee MDPI, Basel, Switzerland. This article is an open access article distributed under the terms and conditions of the Creative Commons Attribution (CC BY) license (<http://creativecommons.org/licenses/by/4.0/>).